

Dynamic effective anisotropy: Asymptotics, simulations, and microwave experiments with dielectric fibers

Lauris Ceresoli,¹ Redha Abdeddaim,¹ Tryfon Antonakakis,² Ben Maling,³ Mohammed Chmiaa,¹ Pierre Sabouroux,¹ Gérard Tayeb,¹ Stefan Enoch,¹ Richard V. Craster,³ and Sébastien Guenneau^{1,*}

¹*Aix-Marseille Université, CNRS, Centrale Marseille, Institut Fresnel, 13013 Marseille, France*

²*Multiwave Technologies AG, Fongit, 1228 Geneva, Switzerland*

³*Department of Mathematics, Imperial College London, London SW7 2AZ, United Kingdom*

(Received 27 October 2014; revised manuscript received 14 October 2015; published 30 November 2015)

We investigate dynamic effective anisotropy in photonic crystals (PCs) through a combination of an effective medium theory, which is a high-frequency homogenization (HFH) method explicitly developed to operate for short waves, as well as through numerical simulations and microwave experiments. The HFH yields accurate predictions of the effective anisotropic properties of periodic structures when the wavelength is of comparable order to the pitch of the array; specifically, we investigate a square array of pitch 2 cm consisting of dielectric rods of radius 0.5 cm and refractive index $n = \sqrt{6}$ within an air matrix. This behaves as an effective medium, with strong artificial anisotropy, at a frequency corresponding to a flat band emerging from a Dirac-like point in transverse magnetic (TM) polarization. At this frequency, highly directive emission is predicted for an electric source placed inside this PC, and this artificial anisotropy can be shown to coincide with a change of character of the underlying effective equation from isotropic to unidirectional, with coefficients of markedly different magnitudes appearing in the effective equation tensor. In transverse electric (TE) polarization, we note a second radical change of character of the underlying effective equation, this time from elliptic to hyperbolic, near a frequency at which a saddle point occurs in the corresponding dispersion curves. Delicate microwave experiments are performed in both polarizations for such a PC consisting of 80 rods, and we demonstrate that a directive emission in the form of a + (respectively, an X) is indeed seen experimentally at the predicted frequency 9.5 GHz in TM polarization (respectively, 5.9 GHz in TE polarization). These are clearly dynamic effects since in the quasistatic regime the PC just behaves as an isotropic medium.

DOI: [10.1103/PhysRevB.92.174307](https://doi.org/10.1103/PhysRevB.92.174307)

PACS number(s): 41.20.Jb, 42.25.Bs, 42.70.Qs, 43.20.Bi

I. INTRODUCTION

Over the past 25 years, many significant advances have created a deep understanding of the optical properties of photonic crystals (PCs) [1–3], which are dielectric periodic structures that prohibit the propagation of light, or allow it only in certain directions at certain frequencies, or localize light in specified regions. However, PCs not only display photonic band gaps but more generally share a complex photonic band structure displaying strong dispersion and anisotropy [4,5] allowing for a number of interesting optical phenomena such as superprism [6], self-collimation [7,8], and ultrarefractive [9] features. Applied mathematicians try to capture the essence of physical phenomena within a microstructured medium through homogenization theories [10]. Unfortunately, these are usually limited to the quasistatic regime and therefore cannot tackle the dynamic effects listed above. A great advantage of homogenization, or effective medium, theories is that they replace a possibly complicated microstructure with a single effective medium, with the relevant physical properties encapsulated by effective parameters in some “averaged” sense. Recently [11], a dynamic homogenization theory has been developed entitled high-frequency homogenization (HFH) that claims to overcome this limitation of homogenization to low frequencies. The HFH theory makes various predictions regarding dynamic anisotropy, which are captured through changes in the coefficients of a frequency-dependent tensor. Our aim is

to explore two such effects and to compare with experiments, thereby validating HFH as an efficient tool for interpretation and design.

To distinguish HFH within the broader area of asymptotic methods, it focuses attention on the physics within a supercell of side-length L , which is the long-scale, and captures the fine details of field oscillations inside a much smaller elementary cell of side length $2l$ [11]. In contrast with classical homogenization theories [10], the wavelength need not be large compared to l in order to perform the asymptotic analysis, as the small parameter $\eta = l/L$ only requires the supercell to be much larger than its constituting elementary cells. HFH is somewhat related to the method of the effective mass tensor, well known in the solid state community [12–14], although we stress that the former contains higher-asymptotic terms. HFH also has connection with abstract mathematical homogenization theories of periodic elliptic operators [15,16].

In this article, we choose a specific photonic crystal arrangement, then apply the asymptotic theory to gain insight into how the anisotropy arises for an electric and a magnetic source placed in its center. The theory gives predictions of both the specific frequency and the shape of the resulting fields in transverse magnetic (TM) and transverse electric (TE) polarizations, which are then investigated through experiment. The experiments confirm directive emission in the form of a + (respectively, an X) in TM (respectively, TE) polarization at a frequency corresponding to a flat band emerging from a Dirac point in TM (respectively, a saddle point in TE) polarization. We are unaware of similar TE and TM experiments for a PC with dielectric fibers.

*sebastien.guenneau@fresnel.fr

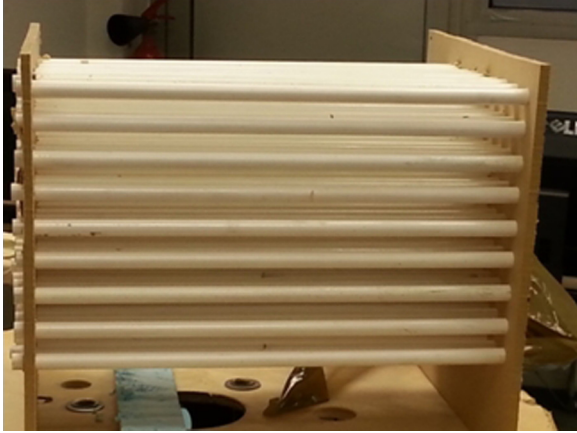


FIG. 1. (Color online) Photo of the dielectric photonic crystal, which consists of 80 parallel dielectric rods inserted in a square array of holes drilled in hardwood plates at either end.

II. MATHEMATICAL SETUP OF THE PHYSICAL PROBLEM

We consider a PC of dielectric fibers assembled as shown in Fig. 1. We use rectangular Cartesian coordinates in space, $(x_1, x_2, x_3) = (\mathbf{x}, x_3)$, with \mathbf{x} the transverse coordinates and x_3 taken along the fiber axes (i.e., perpendicular to the wood plates in Fig. 1).

A. Transverse magnetic (TM) polarization

For the transverse magnetic polarization it is natural to work in terms of the longitudinal electric field $\mathbf{E}(\mathbf{x}) = (0, 0, E_3(\mathbf{x})) \exp(-i\omega t)$, where ω is the angular wave frequency. This time dependence is assumed understood and suppressed henceforth. In this TM polarization time-harmonic solutions of Maxwell's equations satisfy a Helmholtz equation [3]:

$$(\nabla^2 + \omega^2 \varepsilon_r \varepsilon_0 \mu_0) E_3 = 0, \quad (1)$$

where ε_r is the spatially varying relative dielectric permittivity and $\varepsilon_0 \mu_0 = c^{-2}$ with c the speed of light in vacuum. Moreover, $\nabla^2 = \partial_{x_1}^2 + \partial_{x_2}^2$ is the Laplacian in transverse coordinates.

If we consider an infinite doubly periodic medium upon a square lattice then this equation can be supplied with Floquet-Bloch boundary conditions at the edges of a square periodic cell, with side length of say $2l$, given by

$$\begin{aligned} E_3(l, x_2) &= e^{i\kappa_1} E_3(-l, x_2), \\ \partial_{x_1} E_3(l, x_2) &= e^{i\kappa_1} \partial_{x_1} E_3(-l, x_2), \\ E_3(x_1, l) &= e^{i\kappa_2} E_3(x_1, -l), \\ \partial_{x_2} E_3(x_1, l) &= e^{i\kappa_2} \partial_{x_2} E_3(x_1, -l). \end{aligned} \quad (2)$$

This is an essential step in constructing the dispersion curves that characterise wave propagation through the medium and yields the so-called band diagrams [3] as, for instance, shown in Fig. 2. Equations (2) involve the Bloch wave vector $\boldsymbol{\kappa} = (\kappa_1, \kappa_2)$ characterizing the phase shift as one moves from one cell to the next. Restricting our analysis to a piecewise constant dielectric permittivity describing a square array of circular dielectric rods, the Helmholtz Eq. (1) needs to be solved in

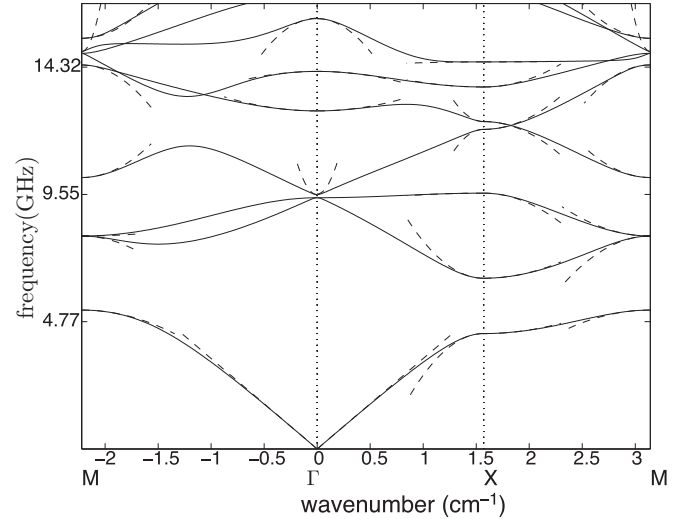


FIG. 2. Floquet-Bloch dispersion curves for a circular dielectric inclusion of radius $r = 0.5$ cm and relative permittivity 6, surrounded by air in a periodic cell of side-length $2l = 2$ cm in TM polarization. Solid curves are from FEM and dashed curves from the asymptotic HFH.

each homogeneous phase within the periodic cell. In addition to the Floquet-Bloch conditions Eq. (2), one has to ensure that E_3 and its Neumann derivative $\nabla E_3 \cdot \mathbf{n}$ are continuous across the circular boundary, where \mathbf{n} is the outward unit normal to the boundary.

B. Transverse electric (TE) polarization

In the transverse electric polarization, we now consider the longitudinal magnetic field $\mathbf{H}(\mathbf{x}) = (0, 0, H_3(\mathbf{x})) \exp(-i\omega t)$ as the unknown and Maxwell's equations then lead to

$$(\nabla^T \varepsilon_r^{-1} \nabla + \omega^2 \varepsilon_0 \mu_0) H_3 = 0, \quad (3)$$

where $\nabla^T = (\partial_{x_1}, \partial_{x_2})$ denotes the transpose of the gradient in transverse coordinates.

The Floquet-Bloch boundary conditions at the edges of the periodic cell are as in Eq. (2) with the unknown E_3 replaced by H_3 . However, in the TE polarization one has to ensure that H_3 and $\varepsilon_r^{-1} \nabla H_3 \cdot \mathbf{n}$ are continuous across the circular boundary, where \mathbf{n} is the outward unit normal to the boundary. The latter boundary conditions are slightly more involved than for the TM case.

III. HIGH-FREQUENCY HOMOGENIZATION

We now describe the essential steps behind the effective medium theory (HFH) we use; the general development is in Ref. [11] with an application to the TM electromagnetic case in Ref. [17] for a doubly periodic array of infinite conducting fibers (Dirichlet inclusions) and in Ref. [18] for three-phase checkerboards.

In the present paper we address the case of dielectric fibers in both TE and TM polarization. The basic idea is that the behavior at the edges of the Brillouin zone, where standing waves occur, encodes information about the local behavior and multiple scattering between the cylinders. This local behavior

is then modulated by a function on the long-scale that satisfies an effective equation. All of this can be made rigorous and the mathematical theory is in Refs. [11,17]. In brief, we consider a square cell, of size $2l$, that repeats to fill a supercell, of size L , which encompasses $(L/2l)^2$ cells within the transverse plane. The discrepancy between scales is used to create a multiple scales approach and we introduce microscopic and macroscopic variables $\xi = \mathbf{x}/l$ and $\mathbf{X} = \mathbf{x}/L$, respectively, and treat ξ, \mathbf{X} as being independent. The longitudinal electric field $E_3(\mathbf{x})$ is written as $E_3(\mathbf{X}, \xi)$, and then expanded in terms of a small parameter $\eta = l/L \ll 1$, so

$$E_3(\mathbf{X}, \xi) = E_3^{(0)}(\mathbf{X}, \xi) + \eta E_3^{(1)}(\mathbf{X}, \xi) + \eta^2 E_3^{(2)}(\mathbf{X}, \xi) + \dots \quad (4)$$

The longitudinal magnetic field is similarly expanded as $H_3(\mathbf{X}, \xi) = H_3^{(0)}(\mathbf{X}, \xi) + \dots$, and the frequency as $\omega^2 = \omega_0^2 + \eta\omega_1^2 + \eta^2\omega_2^2 + \dots$. The leading order solution $E_3^{(0)}(\mathbf{X}, \xi)$ (respectively, $H_3^{(0)}(\mathbf{X}, \xi)$) is associated with a standing wave eigenfrequency ω_0 and is proportional to the associated Bloch eigensolution on the short scale, which we call $U_0^E(\xi)$ (respectively, $U_0^H(\xi)$). This standing wave frequency, which can be high, and the eigensolution, which can oscillate rapidly, are easily found from the usual Bloch analysis that leads to the dispersion curves. The leading-order electric and magnetic fields are then given as

$$\begin{aligned} E_3^{(0)}(\mathbf{x}, \xi) &= f_0^E(\mathbf{X})U_0^E(\xi), \\ H_3^{(0)}(\mathbf{x}, \xi) &= f_0^H(\mathbf{X})U_0^H(\xi), \end{aligned} \quad (5)$$

so the short scale, potentially highly oscillatory, field $U_0^E(\xi)$ (respectively, $U_0^H(\xi)$) is modulated by a long-scale function $f_0^E(\mathbf{X})$ (respectively, $f_0^H(\mathbf{X})$). The key point of the analysis of Ref. [11] is to show that this long-scale field satisfies an effective partial differential equation posed entirely on the long scale:

$$T_{ij}^\alpha \frac{\partial^2}{\partial X_i \partial X_j} f_0^\alpha + \omega_0^2 \varepsilon_0 \mu_0 f_0^\alpha = 0, \quad \text{for } i, j = 1, 2, \quad (6)$$

with the tensor $T_{ij}^\alpha = t_{ij}^\alpha [\int_S \rho^\alpha (U_0^\alpha)^2 dS]^{-1}$. Here, $\alpha = E$ in TM polarization, $\alpha = H$ in TE polarization, and $\rho^E = 1$, $\rho^H = \varepsilon_r$. Furthermore, t_{ij}^α 's are given by annex problems set on the periodic cell with diagonal entries

$$\begin{aligned} t_{ii}^\alpha &= \int_{-l}^l \int_{-l}^l a^\alpha (U_0^\alpha)^2 d\xi_1 d\xi_2 + 2 \int_{-l}^l \int_{-l}^l a^\alpha \partial_{\xi_i} U_{1_i} U_0^\alpha d\xi_1 d\xi_2 \\ &+ \int_{-l}^l \int_{-l}^l \partial_{\xi_i} a^\alpha U_{1_i} U_0^\alpha d\xi_1 d\xi_2, \end{aligned} \quad (7)$$

and off-diagonal entries

$$\begin{aligned} t_{ij}^\alpha &= 2 \int_{-l}^l \int_{-l}^l a^\alpha \partial_{\xi_i} U_{1_j} U_0^\alpha d\xi_1 d\xi_2 \\ &+ \int_{-l}^l \int_{-l}^l \partial_{\xi_i} a^\alpha U_{1_j} U_0^\alpha d\xi_1 d\xi_2 \quad \text{for } i \neq j, \end{aligned} \quad (8)$$

where $a^E = \varepsilon_r^{-1}$ and $a^H = 1$, in TM and TE polarization, respectively. The vector field $\mathbf{U}_1(\xi)$ in Eq. (8) is the solution of a forced Helmholtz equation (see, e.g., Ref. [11]), and appears

within the first-order term of Eq. (4), such that

$$E_3^{(1)}(\mathbf{X}, \xi) = f_1^E(\mathbf{X})U_0^E(\xi; \Omega_0) + \nabla_{\mathbf{x}} f_0^E(\mathbf{X}) \cdot \mathbf{U}_1^E(\xi), \quad (9)$$

for $\alpha = E$, and likewise when $\alpha = H$ with $H_3^{(1)}(\mathbf{X}, \xi)$.

The short scale is completely encoded within the tensor T_{ij}^α , which takes numerical values dependent upon the geometry, material parameters, and standing wave frequency; crucially it does depend upon ω_0 (which obviously is different in TE and TM polarizations) and so captures dynamic effects. Equation (6) encapsulates the dynamic effective anisotropy of the photonic crystal through the tensor T_{ij}^α ; its detailed derivation can be found in Refs. [11,17], and an interpretation of T_{ij}^α in terms of effective media is in Ref. [18]. There are some subtleties associated with repeated eigenvalues that occur when dispersion branches cross at a standing wave frequency. In such cases Eq. (6) requires modification as detailed in Ref. [17]. Note that there is no summation over repeated indices for the t_{ii}^α term. In the piecewise-constant case, the structure of T_{ij}^α depends strongly on the boundary conditions associated with the inclusions; the results here, for instance, are markedly different in the TE and TM cases, and also from those of the Neumann and Dirichlet [17] cases corresponding to perfecting inclusions in either polarization.

As we shall demonstrate, changes in the components of T_{ij}^α from positive to near zero or negative correspond to changes in the behavior of the effective medium, and we can use this understanding to interpret, and more importantly predict, when specific physical effects might occur. Notably, the possible transition to hyperbolic behavior [17] is reminiscent of recent work on hyperbolic-like metamaterials [19–25].

IV. FEM VERSUS HFH DISPERSION CURVES FOR STRUCTURED DIELECTRIC FIBERS

We now focus on the specific case of a dielectric rod of relative permittivity 6 and radius 0.5 cm, surrounded by air in a square cell of side-length $2l = 2$ cm. This constitutes a good model for one elementary cell of the PC shown in Fig. 1. Initially we imagine an infinite structure made from a doubly periodic array of this cell, thereby enabling us to apply Floquet-Bloch conditions and hence draw band diagrams that can display interesting features such as vanishing or negative group velocity and band gaps in the transverse plane.

A. TM polarization

Figure 2 shows the resulting dispersion curves computed with finite elements (solid curves) and those obtained from HFH (dashed curves) in transverse magnetic polarization. We notably observe some missed crossing between the second, third, and fourth curves at Γ point, which is reminiscent of Dirac points in arrays of constrained (Dirichlet) points [17]. We note that arrays of thin metal wires were studied in the '90s in conjunction with zero-frequency band gaps and noncommuting limits [26].

The HFH curves result from asymptotics around the points Γ , X , and M , and so are highly accurate there, which in itself is a useful cross-verification of the effective medium methodology. Incidentally, one can extend the domain of validity by working with an elementary cell of 2×2 cylinders

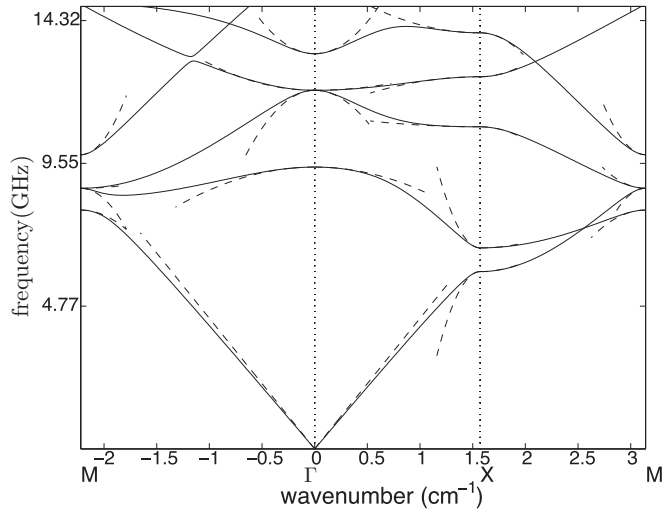


FIG. 3. Floquet-Bloch dispersion curves in TE polarization for same PC parameters as described in the caption of Fig. 2. Solid curves are from FEM and dashed curves from the asymptotic HFH.

and then one gets asymptotics along the middle of, say, the path ΓM (see Ref. [17]). At this point some brief explanation is required of the wave-number axis. In wave-number space the Brillouin zone is a square, but the symmetry of the cell allows us to treat an irreducible Brillouin zone, which is a triangle joining the points $\Gamma = (0,0)$, $X = (\pi/2,0)$, and $M = (\pi/2,\pi/2)$. As is conventional we show the dispersion curves for wave numbers taken around the edge of this triangle ΓXM .

From Fig. 2 we see that a photonic band gap exists in TM polarization, and this is known to allow for microcavity effects if one makes a defect in the photonic crystal [27]. Further effects can also be predicted from the dispersion curves; for instance, one can achieve slow light [28] effects at symmetry points of the Brillouin zone, where the slope of the dispersion curves is zero. The behavior at the edges of the Brillouin zone is key to interpreting the band diagram.

B. TE polarization

There is a radical change in the band structure when we consider the other polarization case. From Fig. 3 we note that the stop band is no longer present in TE polarization, and nor is the near-Dirac cone. So, at first sight, one might say the TM polarization seems to be more prone to interesting physical effects. However, as we shall demonstrate the PC behaves like a hyperbolic-type metamaterial near the frequency 5.9 GHz (1st mode at X), at which a saddle point exists in TE polarization. We note in passing that interesting physical phenomena occur near saddle points, such as diverging density of states [19,29–32], and this could be investigated with HFH theory, but this goes beyond the scope of the present paper.

V. FEM VERSUS HFH MODES FOR PHOTONIC CRYSTAL

It is interesting to approximate the dispersion curves with HFH theory. The resulting curves are shown as dashed lines in Figs. 2 and 3. Classical homogenization can only capture the

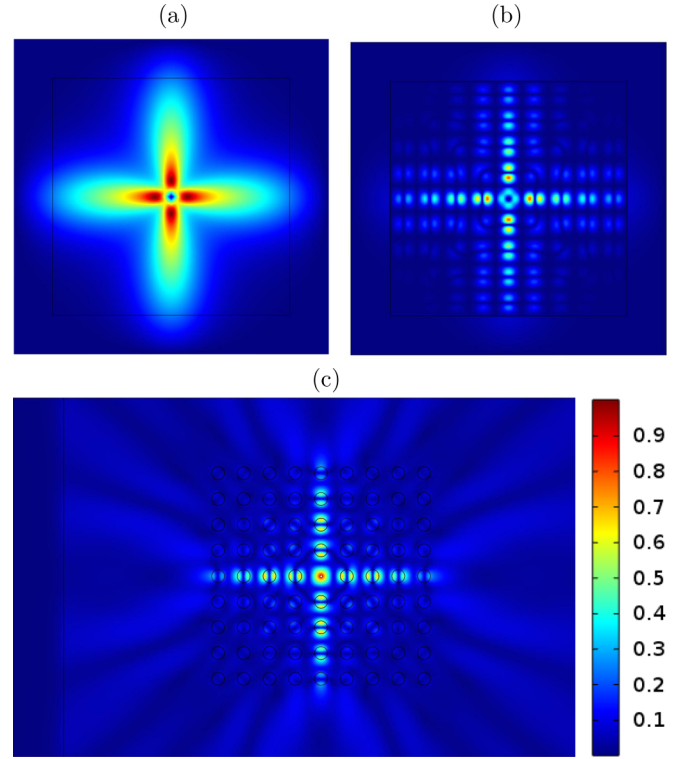


FIG. 4. (Color online) The modulus of the longitudinal electric field, E_3 , for a line source at 9.5 GHz placed in the center of a PC with properties as described in the caption of Fig. 2: Panels (a) and (b) show Comsol multiphysics computations using the effective medium (HFH) theory where the T_{ij}^E are for the 3rd mode at X , which are $T_{11}^E = -0.1548$, $T_{22}^E = -1.7773$, and $T_{12}^E = T_{21}^E = 0$. Panel (a) shows only the long-scale component $|f_0^E|$ and (b) shows the leading order asymptotic solution $|E_3^{(0)}(\mathbf{x}, \xi)|$. In both panels the computational region is surrounded by a layer of perfectly matched layers (to prevent artificial reflections due to the truncation of an infinite domain), which is outside the lines in these panels. Panel (c) shows the full Comsol simulation using the Helmholtz Eq. (1). Clearly the agreement of asymptotic and full computation is excellent both qualitatively and quantitatively. Color scale is linear.

effective linear curves near the origin at the Γ point, whereas HFH neatly approximates the solid curves, computed with finite elements, even in the stop-band range of frequencies. Departures from the solid curves away from the Γ , X , and M points can be resolved by considering higher-symmetry points in the first Brillouin zone [17].

A. TM polarization

The effective medium methodology allows us to investigate a whole class of exotic effective behaviors associated with slow modes, with the T_{ij}^E coefficients encoding this information. For instance, near the X symmetry point in Fig. 2, one gets a mode (the third mode at 9.5 GHz) that displays strong dynamic anisotropy as $|T_{11}^E| \ll |T_{22}^E|$ with $T_{12}^E = T_{21}^E = 0$; the values are $T_{11}^E = -0.1548$, $T_{22}^E = -1.7773$. This anisotropy leads to the highly directive radiative pattern observed in the full computations of Fig. 4(c), reminiscent of self-collimation in scattering problems with photonic crystals. Computations using the effective theory in Fig. 4(b) are remarkably accurate,

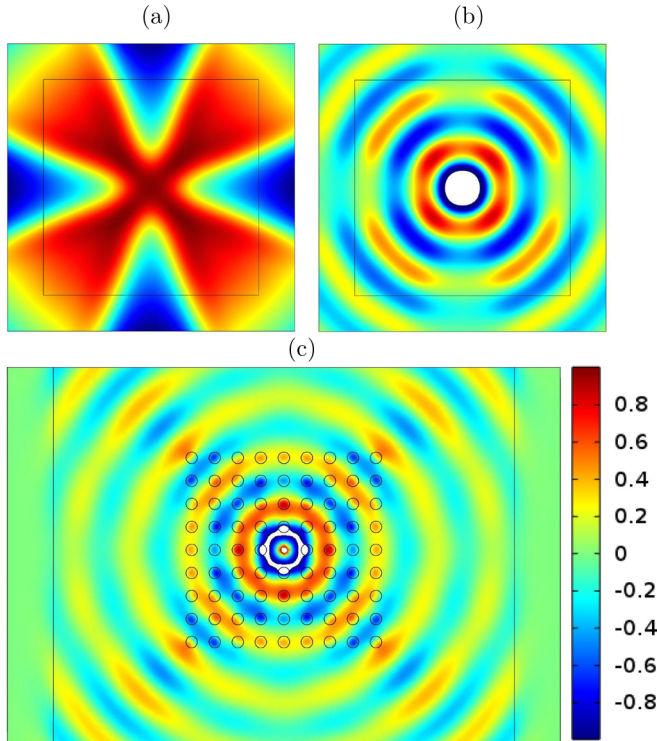


FIG. 5. (Color online) The longitudinal magnetic field, H_3 , for a line source at 5.9 GHz placed in the center of a PC with properties as described in the caption of Fig. 2: Panels (a) and (b) show Comsol multiphysics computations using the effective medium (HFH) theory where the T_{ij}^H are for the 1st mode at X, which are $T_{11}^H = -8.6656$, $T_{22}^H = 0.9209$, and $T_{12}^H = T_{21}^H = 0$. Panel (a) shows only the modulus of the long-scale component f_0^H and (b) shows the real part of leading order asymptotic solution $H_3^{(0)}(\mathbf{x}, \xi)$. In both panels the computational region is surrounded by a layer of perfectly matched layers (to prevent artificial reflections due to the truncation of an infinite domain), which is outside the lines in these panels. Panel (c) shows the real part of H_3 from full Comsol simulation using the Helmholtz Eq. (1). Clearly the agreement of asymptotic and full computation is excellent both qualitatively and quantitatively. Color scale is linear.

and the magnitude of the long-scale modulation function f_0^E is shown in Fig. 4(a). One can accurately predict using the asymptotic theory that this highly directional behavior will exist from the evident anisotropy of the tensor T_{ij}^E . Another key advantage of having an effective theory, valid for high frequencies, is that the computations for the effective equation are an order of magnitude faster than those of full computations for the microstructured medium.

B. TE polarization

Self-collimation is not the only directional anisotropy that can arise in the PC. In the other polarization case, we achieve an X-shaped emission when $T_{11}^H T_{22}^H < 0$, in which case the effective Eq. (6) describes that of a hyperbolic-like metamaterial [33]. Here again HFH reproduces almost perfectly the emission of a magnetic source inside the PC computed with finite elements. This striking effect is shown

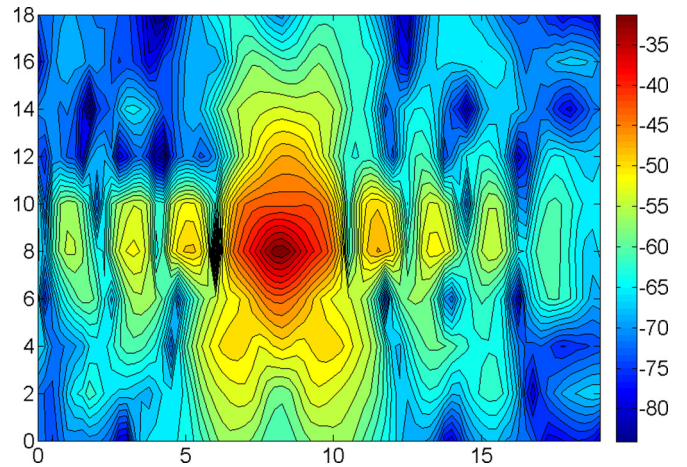


FIG. 6. (Color online) Result of microwave experiments for an electric source (TM polarization) at 9.5 GHz placed in the center of the PC. Color scale is in dB.

in Fig. 5. For simple geometries some gap-edge asymptotics of defect modes can also be derived using a Green’s function approach [34].

VI. MICROWAVE EXPERIMENTS

Now that we have HFH at our disposal as a design tool, we can use it interactively with experiments to find the key operating frequencies and material parameters for directivity, among other effects. The predictions described thus far are now explored with a novel set of experiments. In Figs. 6 and 7, we show experimental measurements for the photonic crystal designed and characterized at the Institut Fresnel. The structure shown in Fig. 1 is a PC of square symmetry made of 80 dielectric rods (a 9×9 array with the central rod removed). The rods consist of alumina powder and synthetic resin, are 0.5 cm in radius and 300 mm in length, and their relative permittivity was shown to be equal on average to 6

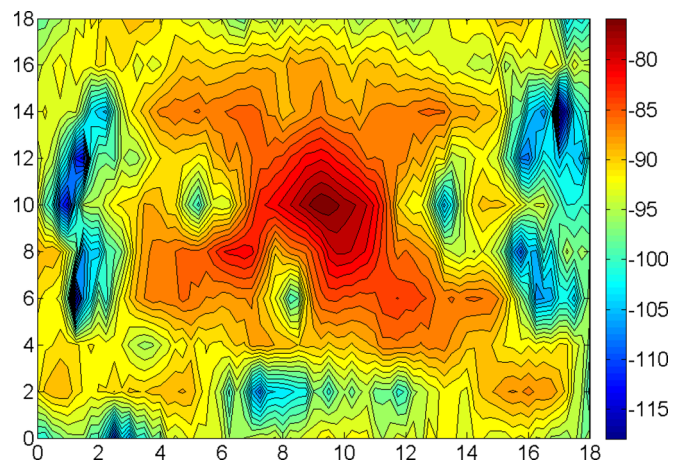


FIG. 7. (Color online) Result of microwave experiments for a magnetic source (TE polarization) at 5.9 GHz placed in the center of the PC. Color scale is in dB.

(with up to 5 percent of inaccuracy) in Ref. [27]. This is the experimental analogue of that used in the theory, except that the computations for Figs. 4 and 5 are planar, corresponding to the limiting case of infinitely long fibers, whereas the experiments are three-dimensional; hence the discrepancy in Fig. 6 (respectively, Fig. 7) versus those of Fig. 4 (respectively, Fig. 5). Nonetheless, the directional anisotropy found in the experiments is clear.

Figure 6 shows the modulus of the longitudinal component of the electric field, $|\text{Re}(E_3)|$, inside the crystal at the frequency corresponding to that used in Fig. 4. This component is carefully measured with a vectorial network analyzer using a monopole probe when a small monopole antenna is located at the center of the structure. To ensure excitation and measurement of the component E_3 , both the emitting monopole and the probe are aligned with the axis parallel to the fibers. Simulations and measurements are indeed in excellent agreement. The longitudinal electric field E_3 in the two scanned direction (x_1, x_2) is maximal along the central lines (horizontal and vertical), making a cross as predicted by HFH.

In the same way, Fig. 7 shows the modulus of the longitudinal component of the magnetic field, $|\text{Re}(H_3)|$, inside the crystal at the frequency corresponding to that used in Fig. 5. We now use a magnetic probe for excitation and measurement of H_3 , with the emitting monopole and the probe aligned along the axes of these fibers. Simulations and measurements are once again in excellent agreement. The longitudinal magnetic field H_3 is maximal along the diagonal lines, making an X as predicted by HFH.

VII. CONCLUSION AND APPLICATIONS

In this article, we have experimentally tested an effective medium formulation for dielectric photonic crystals in transverse magnetic (TM) and transverse electric (TE) polarization, which is not constrained to the low-frequency limit. This is an important step as this theory is now ideally placed to play a role in practical interpretation and design. The HFH methodology captures the dynamic nature of the anisotropy through the tensor T_{ij} , and unveils dynamic anisotropy at critical frequencies, which leads to directive emission either along the x_1 and x_2 axes (in TM polarization) or the diagonals (in TE polarization). In the former case the directive effect comes from an effective tensor with a vanishing eigenvalue, while in the latter case, the eigenvalues have opposite sign, indicating a hyperbolic-type effective equation. Finally, Eqs. (1) and (3) can be used to model problems of pressure acoustic, or antiplane shear, waves with the density, bulk modulus, and shear modulus playing the role of the permittivity. This suggests similar ultradirective emission could be observed with arrays of fibres in other wave areas.

ACKNOWLEDGMENTS

R.V.C. thanks the Engineering Physical Science Research Council (UK) for support through research Grant No. EP/J009636/1 and programme Grant No. EP/L024926/1. P.S., R.A., S.E., and S.G., acknowledge a PEPS CNRS (France) grant Cloaking Externe. S.G. is thankful for an European Research Council grant Anamorphism No. 279673.

-
- [1] E. Yablonovitch, *Phys. Rev. Lett.* **58**, 2059 (1987).
 - [2] S. John, *Phys. Rev. Lett.* **58**, 2486 (1987).
 - [3] J. Joannopoulos, S. Johnson, J. Winn, and R. Meade, *Photonic Crystals, Molding the Flow of Light* (Princeton University Press, Princeton, NJ, 2008).
 - [4] P. S. J. Russell, *Appl. Phys. B* **39**, 231 (1986).
 - [5] R. Zengerle, *J. Mod. Opt.* **34**, 1589 (1987).
 - [6] H. Kosaka, T. Kawashima, A. Tomita, M. Notomi, T. Tamamura, T. Sato, and S. Kawakami, *Phys. Rev. B* **58**, R10096(R) (1998).
 - [7] H. Kosaka, T. Kawashima, A. Tomita, M. Notomi, T. Tamamura, T. Sato, and S. Kawakami, *Appl. Phys. Lett.* **74**, 1212 (1999).
 - [8] D. Chigrin, S. Enoch, C. S. Torres, and G. Tayeb, *Opt. Express* **11**, 1203 (2003).
 - [9] B. Gralak, S. Enoch, and G. Tayeb, *J. Opt. Soc. Am. A* **17**, 1012 (2000).
 - [10] G. W. Milton, *The Theory of Composites* (Cambridge University Press, Cambridge, 2002).
 - [11] R. V. Craster, J. Kaplunov, and A. V. Pichugin, *Proc. R. Soc. London A* **466**, 2341 (2010).
 - [12] S. Pekar, *Zh. Eksp. Teor. Fiz.* **16**, 933 (1946).
 - [13] J. M. Luttinger, *Phys. Rev.* **97**, 869 (1955).
 - [14] G. H. Wannier, *Phys. Rev.* **52**, 191 (1937).
 - [15] G. Allaire, and A. Piatnitski, *Commun. Math. Phys.* **258**, 1 (2005).
 - [16] M. S. Birman and T. A. Suslina, *J. Math. Sci.* **136**, 3682 (2006).
 - [17] T. Antonakakis, R. Craster, and S. Guenneau, *New J. Phys.* **15**, 103014 (2013).
 - [18] R. V. Craster, J. Kaplunov, E. Nolde, and S. Guenneau, *J. Opt. Soc. Am. A* **28**, 1032 (2011).
 - [19] W. Yan, M. Wubs, and N. A. Mortensen, *Phys. Rev. B* **86**, 205429 (2012).
 - [20] D. Schurig and D. Smith, *Appl. Phys. Lett.* **82**, 2215 (2003).
 - [21] Z. Jacob, L. Alekseyev, and E. Narimanov, *Opt. Express* **14**, 8247 (2006).
 - [22] I. Smolyaninov, Y.-J. Hung, and C. Davis, *Science* **315**, 1699 (2007).
 - [23] M. Noginov, Y. Barnakov, G. Zhu, T. Tumkur, H. Li, and E. Narimanov, *Appl. Phys. Lett.* **94**, 151105 (2009).
 - [24] L. M. Custodio, C. T. Sousa, J. Ventura, J. M. Teixeira, P. V. S. Marques, and J. P. Araujo, *Phys. Rev. B* **85**, 165408 (2012).
 - [25] C. Simovski, P. Belov, A. Atrashchenko, and Y. Kivshar, *Adv. Mater.* **24**, 4229 (2012).
 - [26] N. A. Nicorovici, R. C. McPhedran, and L. C. Botten, *Phys. Rev. Lett.* **75**, 1507 (1995).
 - [27] P. Sabouroux, G. Tayeb, and D. Maystre, *Opt. Commun.* **160**, 33 (1999).

- [28] A. Figotin and I. Vitebskiy, [Waves Random Complex Media](#) **16**, 293 (2006).
- [29] L. V. Hove, [Phys. Rev.](#) **89**, 1189 (1953).
- [30] O. D. Miller, S. G. Johnson, and A. W. Rodriguez, [Phys. Rev. Lett.](#) **112**, 157402 (2014).
- [31] H. Krishnamoorthy, Z. Jacob, E. Narimanov, I. Kretzschmar, and V. Menon, [Science](#) **336**, 205 (2012).
- [32] Z. Jacob, J.-Y. Kim, G. Naik, A. Boltasseva, E. Narimanov, and V. Shalaev, [Appl. Phys. B](#) **100**, 215 (2010).
- [33] A. Poddubny, I. Iorsh, P. Belov, and Y. Kivshar, [Nat. Photonics](#) **7**, 948 (2013).
- [34] K. B. Dossou, L. C. Botten, R. C. McPhedran, A. A. Asatryan, and C. Martijn de Sterke, [Opt. Express](#) **15**, 4753 (2007).